Variabilities in the polar field and solar cycle due to irregular properties of Bipolar Magnetic Regions

Pawan Kumar⋆, Bidya Binay Karak†, Anu Sreedevi‡

Department of Physics, Indian Institute of Technology (Banaras Hindu University), Varanasi 221005, India

ABSTRACT

Decay and dispersal of the tilted Bipolar Magnetic Regions (BMRs) on the solar surface are observed to produce the large-scale poloidal field, which acts as the seed for the toroidal field and, thus, the next sunspot cycle. However, various properties of BMR, namely, the tilt, time delay between successive emergences, location, and flux, all have irregular variations. Previous studies show that these variations can lead to changes in the polar field. In this study, we first demonstrate that our 3D kinematic dynamo model, STABLE, reproduces the robust feature of the surface flux transport (SFT) model, namely the variation of the generated dipole moment with the latitude of the BMR position. Using STABLE in both SFT and dynamo modes, we perform simulations by varying the individual properties of BMR and keeping their distributions the same in all the cycles as inspired by the observations. We find that randomness due to the distribution in either the time delay or the BMR latitude produces negligible variation in the polar field and the solar cycle. However, randomness due to BMR flux distribution produces substantial effects, while the scatter in the tilt around Joy's law produces the largest variation. Our comparative analyses suggest that the scatter of BMR tilt around Joy's law is the major cause of variation in the solar cycle. Furthermore, our simulations also show that the magnetic field-dependent time delay of BMR emergence produces more realistic features of the magnetic cycle, consistent with observation.

Key words: Sun: magnetic fields – dynamo – physical data and process – Sun: sunspots – Sun: activity – Sun: interior

1 INTRODUCTION

The 11-year magnetic cycle in the sun is not regular. The extreme variation in the cycle can be seen as grand minima such as the Maunder minimum and grand maxima namely the modern maximum (Solanki et al. 2004; Svalgaard 2013; Usoskin 2017; Biswas et al. 2023a). Besides this long-term modulation, there are short-term (6 – 18 months) variations which are so-called bursts of activity or seasons of the sun (Rieger et al. 1984; Gurgenashvili et al. 2016) and the double peaks (Karak et al. 2018) in the solar cycle. In addition to the cycle strength, the duration also varies in each cycle. Waldmeier (1935) reported that the strong cycles take less time to rise and vice versa (also see Karak & Choudhuri 2011; Cameron & Schüssler 2016). Hence, the variation in the amplitude and duration of the cycle is somewhat related. Further, the time of reversal of the polar field of the sun is also not fixed, and it differs from cycle to cycle by a few months to years. In fact, there are evidences of possible triple reversals of the polar field (Makarov et al. 1983; Mordvinov et al. 2022). Because of this variable nature of the solar cycle, it is challenging to make a prediction of the future solar cycle (Petrovay 2020; Bhowmik et al. 2023). However, prediction is compelling because the solar magnetic cycle affects the heliosphere, thus our technology-dependent society (Temmer 2021).

It is believed that the solar magnetic cycle is the result of a dynamo operating in the solar convection zone (CZ) and thus the variability observed in the solar cycle must be connected to the dynamo action (Karak 2023). There are enough evidences that the solar dynamo is of $\alpha\Omega$ type (Karak et al. 2014; Cameron & Schüssler 2015; Charbonneau 2020) in which the α denotes the generation of poloidal field from the toroidal one (the α effect) and the Ω represents the Ω effect in which the toroidal field is generated from the poloidal one through the differential rotation. Since the idea of Babcock (1961) and Leighton (1964), it has been observed that the tilted bipolar magnetic regions (BMRs) decay and disperse on the solar surface and produce large-scale poloidal field in the Sun (Dasi-Espuig et al. 2010; Kitchatinov & Olemskoy 2011). Hence, we shall consider this Babcock–Leighton process for the generation of the poloidal field in our solar dynamo model. The poloidal field generated near the surface at low latitudes through the Babcock–Leighton process is advected towards the high latitudes and further to the deep CZ with the help of meridional flow, where the Ω effect stretches the poloidal field to give rise to the toroidal field. This toroidal field due to magnetic buoyancy emerges on the solar surface in the form of BMRs (Parker 1955).

In the solar dynamo model, the Babcock–Leighton process is a crucial component which involves randomness. The extensive randomness arises in the Babcock–Leighton process through the tilt angle of BMR. The tilt angle of BMR is observed to increase statistically with the increase of the latitude, which is known as Joy's law (Hale et al. 1919). Observations also show that there is a considerable amount of scatter in tilt angle around this Joy's law (Howard

⋆ E-mail: pawan.kumar.rs.phy18@itbhu.ac.in
† E-mail: karak.phy@itbhu.ac.in
‡ E-mail: anubsreedevi.rs.phy20@itbhu.ac.in

1991; Jha et al. 2020). While in most of the previous studies, the tilt is measured from the sunspot group (when magnetograms data are not available; Sivaraman et al. 2007) or BMR by repeatedly observing the same feature (e.g., McClintock & Norton 2016), recently Sreedevi et al. (2023) have tracked the BMRs for the last two solar cycles and produced unique tilt for each BMR during this period. Figure 2 of Sreedevi et al. (2024) shows Joy's law and the scatter around the tilt obtained from those tracked BMRs. Observations show that the slope of Joy's law has some cycle-to-cycle variation, which can lead to some change in the polar field as demonstrated by Baumann et al. (2004). However, the observed large scatter in the tilt around Joy's law is another major cause of fluctuations in the poloidal field (Jiang et al. 2014; Karak & Miesch 2017; Lemerle & Charbonneau 2017). Furthermore, observations show that about 8% of BMRs in a solar cycle are anti-Hale (McClintock et al. 2014) while 25 to 30% are anti-Joy. These anti-Hale and anti-Joy BMRs produce opposite polarity field and thus they disturb the regular polar field (Cameron et al. 2013; Jiang et al. 2014, 2015; Karak & Miesch 2018; Kitchatinov et al. 2018; Karak et al. 2018; Mordvinov et al. 2022; Pal et al. 2023). Nagy et al. (2017) showed that in the extreme case, a sufficiently complex wrongly tilted (rogue) BMRs can considerably disturb the dynamo and it even may lead to a grand minimum.

The other sources of irregularity in the solar dynamo are the time delay in the BMR emergence, latitudinal position, and the flux of BMR. It has been observed that the time delay between two successive BMRs is not the same, and it follows a distribution. Again from the tracked BMRs from MDI and HMI for the last two solar cycles (Sreedevi et al. 2023), as presented in Fig. 2(a), we find that the lag between two successive BMR emergences follow a distribution which can be approximated by a log-normal distribution. This distribution in the time delay of BMR emergence can introduce a variation in the solar cycle. A related time delay in the solar dynamo is the delay in the rise of the BMR-forming toroidal flux tube from the base of the CZ to the surface; see Sects. 5.3 and 6.4 of Karak (2023). When this delay is magnetic field dependent, it can lead to a variation in the solar cycle (Jouve et al. 2010). Furthermore, the latitude of BMR emergence on the solar surface is also not uniform and plays a role in determining the strength of the polar field (Baumann et al. 2004; Nagy et al. 2017). In fact, Jiang et al. (2015) had shown that an anomalous BMR (anti-Hale or anti-Joy) appearing at low latitude produces a significant change in the dipole moment. The mean latitudes of BMRs in a cycle depend on its strength; in the strong cycles, BMRs begin at high latitudes (Waldmeier 1955; Solanki et al. 2008; Jiang et al. 2014; Mandal et al. 2017). Baumann et al. (2004) showed the photospheric magnetic field at solar minimum decreases with the increase of the mean latitude of the BMR band. Finally, the flux content in the erupting BMR is not constant, and it randomly varies roughly in the range of 10^{21} to 10^{23} Mx following a log-normal distribution as seen in Fig. 2(b); also see Sheeley (1966). Variation in the BMR flux can cause a change in the poloidal field.

Since the polar magnetic field or its proxy is strongly correlated with the activity level of the next cycle (Schatten et al. 1978; Choudhuri et al. 2007; Wang & Sheeley 2009; Kitchatinov & Olemskoy 2011; Muñoz-Jaramillo et al. 2013; Priyal et al. 2014; Kumar et al. 2021, 2022), the variation of the polar field can cause a variation in the solar magnetic cycle. Therefore, to realize the behavior of the future solar cycle, it is essential to understand the polar field of the present cycle.

The variations that we are considering are essentially caused by the stochastic nature of the convection. However, there is an extensive literature elucidating the long-term variability due to nonlinearities arising from the Lorentz feedback of the magnetic field on the flows

(e.g., Tobias et al. 1998; Beer et al. 1998; Weiss & Tobias 2016; Charbonneau 2020; Karak 2023). However, nonlinearities do not always produce variation in the solar cycle. Some of the nonlinearities recognized in the Babcock–Leighton type dynamo models, such as the flux loss through magnetic buoyancy (Biswas et al. 2022), latitude quenching (Jiang 2020; Karak 2020), magnetic field dependent tilt (so-called the tilt quenching Dasi-Espuig et al. 2010; Jha et al. 2020; Sreedevi et al. 2024), inflows around active regions (Martin-Belda & Cameron 2017; Nagy et al. 2020; Teweldebirhan et al. 2024) all have tendency of stabilizing the magnetic field rather than producing large variations in the solar cycle; see Sec. 6.1 of Karak (2023) for a detailed discussion.

In this work, we shall only focus on the long-term variability in the solar cycle due to stochastic forcing caused by the convection on different parameters of Babcock–Leighton process, particularly the irregular properties of BMR. We shall make comparative analyses of the variations of the polar field generated in a cycle arise by the randomness due to the distributions of (i) the time delay of successive BMR eruptions, (ii) the BMR flux, (iii) the BMR tilt angle, and (iv) the latitude of BMR eruption. Our studies differs from the previous ones who have also studied the effect of irregular properties of BMRs. For example, (i) Baumann et al. (2004) who studied the effect of the change of the polar field with the BMR flux distribution profile and shifting the mean latitude and width of the sunspot band, and the slope of Joy's law, (ii) Nagy et al. (2017) who studied the effect of single rough BMR on the operation of the dynamo at different latitudes. (iii) Pal et al. (2023) who showed the effect of anomalous (anti-Hale (anti-Joy), anti-Joy (Hale) and anti-Hale (Joy)) BMRs (5–10% of the total flux) at different phases of the cycles with different latitudes. (iv) Cameron et al. (2016) and Bhowmik & Nandy (2018) who studied the uncertainty in estimating the dipole moment and predicting the cycle strength by including the variability in BMR tilt, latitude and flux.

Further, we shall perform simulations using synthetic BMR data of solar cycles deposited in our 3D kinematic dynamo model STABLE (Surface Flux Transport and Babcock–Leighton) and analyze the polar field and solar cycle variation.

2 MODEL

In the present work, we have used a 3D kinematic dynamo model STABLE (Miesch & Dikpati 2014; Miesch & Teweldebirhan 2016; Hazra et al. 2017; Karak & Miesch 2017). In this model, BMRs are deposited based on the toroidal magnetic field present at the base of CZ, and the decay and dispersal of BMRs near the surface produce the poloidal field. The poloidal field eventually gives rise to the toroidal one through differential rotation and sustains the dynamo loop. This model can also be operated as a surface flux transport (SFT) model if we deposit BMRs on the solar surface. Karak & Miesch (2018) showed that this model also produces the correct latitude-dependent variation of the polar field—higher the latitude of BMR emergence, lower is the polar field generated. Karak (2020) showed that this effect leads to so-called latitude quenching which was suggested by Petrovay (2020); Jiang (2020) based on the SFT model and observation.

To demonstrate the performance of the STABLE model as SFT explicitly, we present the axial dipole moment (DM) produced from a BMR deposited at different latitudes in Fig. 1. We observe that the STABLE model also captures the behavior as seen in SFT model, namely, with increasing the latitude of the BMR emergence, the generation of DM decreases (Fig. 1(a)) and the final saturated dipole
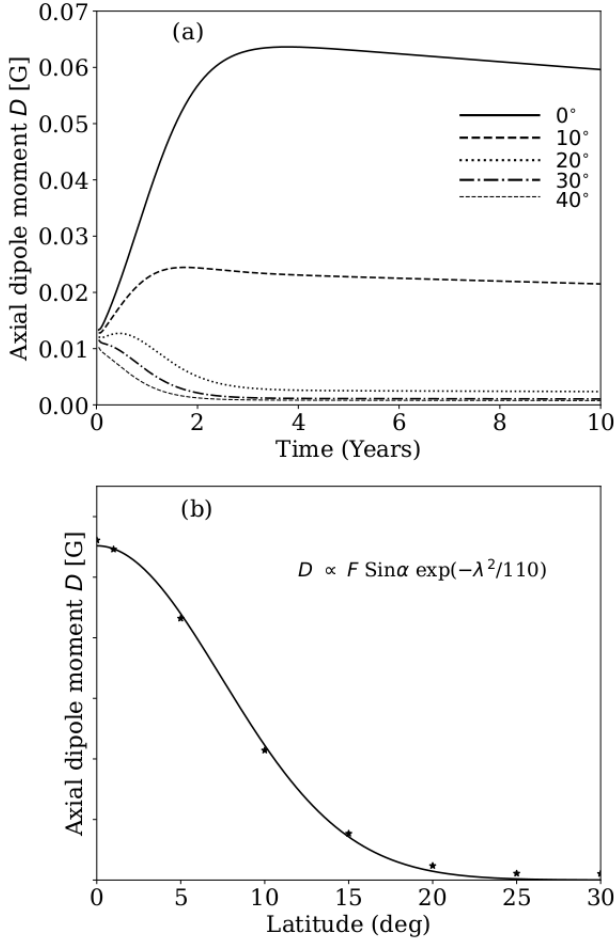
Figure 1. The results produced from STABLE operating in SFT mode. (a) Time evolution of the axial dipole moment (D) of a BMR deposited at different latitudes with constant flux (F) of 10^{22} Mx and tilt (α) of $80°$. (b) The values of the saturated (final) dipole moment vs the latitude of single BMR. The solid curve is the Gaussian profile of the form $\exp(-\lambda^2/110)$ as predicted by the SFT model of Jiang et al. (2014).
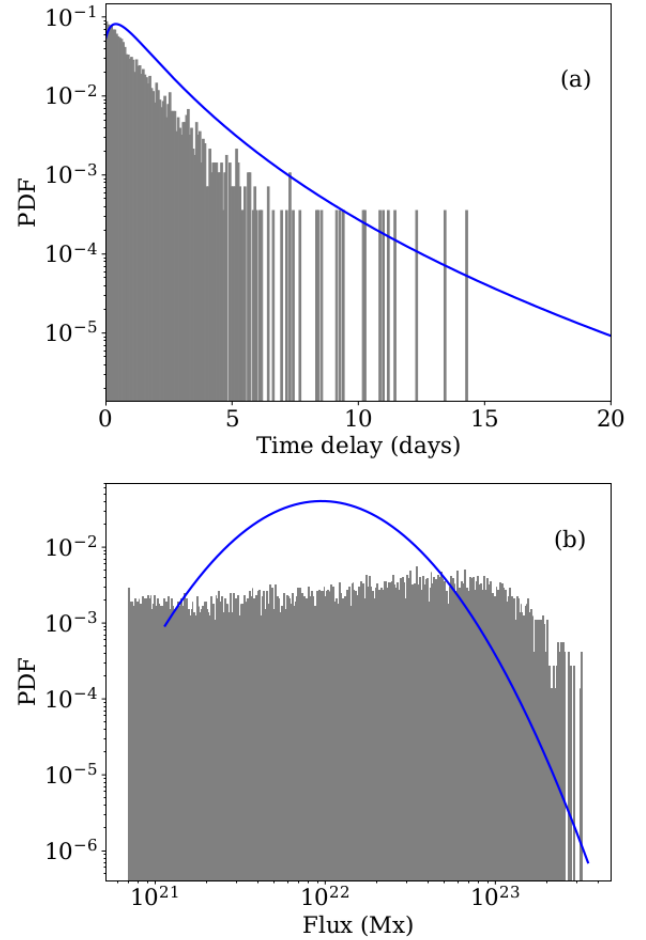

Figure 2. Distributions of (a) the time delay between two successive BMR emergences and (b) flux content of 8800 BMRs obtained from MDI and HMI magnetograms during 1996–2020. These quantities are obtained by tracking each BMR throughout its lifetime or disk passage and taking the average values during the time when the flux is above 70% of its maximum (Sreedevi et al. 2023). The solid lines are the log-normal distributions that approximately fit the data and are used in our (and Karak & Miesch (2017)) calculations.

moment produced can be approximated by a Gaussian profile as predicted by the SFT models (Jiang et al. 2014; Petrovay et al. 2020). We would like to mention that Hazra et al. (2017) failed to capture this feature as they did not include a downward pumping which is essential to make the model consistent with observations and SFT models (Cameron et al. 2012; Karak & Cameron 2016).

In the present study, we shall exploit this feature of the STABLE dynamo model and utilize it as a dynamo simulator to study the solar cycle variation and as an SFT model to study the polar field evolution. One advantage of using STABLE for our study is that we can use the same model in two modes, namely, SFT to study the surface behaviour of magnetic field and dynamo to study the global internal dynamics of fields. In the next subsection, we first describe the STABLE model.

2.1 STABLE model

In this model, we solve the Induction equation in three dimensions (r, θ, ϕ) for the whole CZ with $0.69R \leq r \leq R$ (R is the radius of

the sun), $0 \leq \theta \leq \pi$, and $0 \leq \phi \leq 2\pi$.

$$\frac{\partial \boldsymbol{B}}{\partial t} = \boldsymbol{\nabla} \times \left[(\boldsymbol{V} + \boldsymbol{\gamma}) \times \boldsymbol{B} - \eta_t \boldsymbol{\nabla} \times \boldsymbol{B} \right], \tag{1}$$

where $\boldsymbol{V}$ is the velocity field such that

$$\boldsymbol{V} = v_r(r, \theta)\hat{r} + v_\theta(r, \theta)\hat{\theta} + r \sin \theta \Omega(r, \theta)\hat{\phi}. \tag{2}$$

Here the axisymmetric velocity field is composed of meridional circulation v_r, v_θ, and the differential rotation ($\Omega = v_\phi/r \sin \theta$). The profile of Ω used in this model roughly captures the observed properties as inferred through helioseismology (Schou et al. 1998) and was used in Karak & Miesch (2017). For the meridional circulation, we have considered a single cell circulation profile as used in Karak & Cameron (2016). In equation (1), γ represents the magnetic pumping which helps to suppress the loss of the toroidal field through the surface and thus boosts the dynamo efficiency even at high diffusivity (Cameron et al. 2012; Karak & Cameron 2016). Our model includes a radially downward magnetic pumping of speed 20 m s^{-1} in the near-surface layer ($r \geq 0.9R$) of the sun. In this model, we have considered a radial-dependent effective turbulent diffusivity
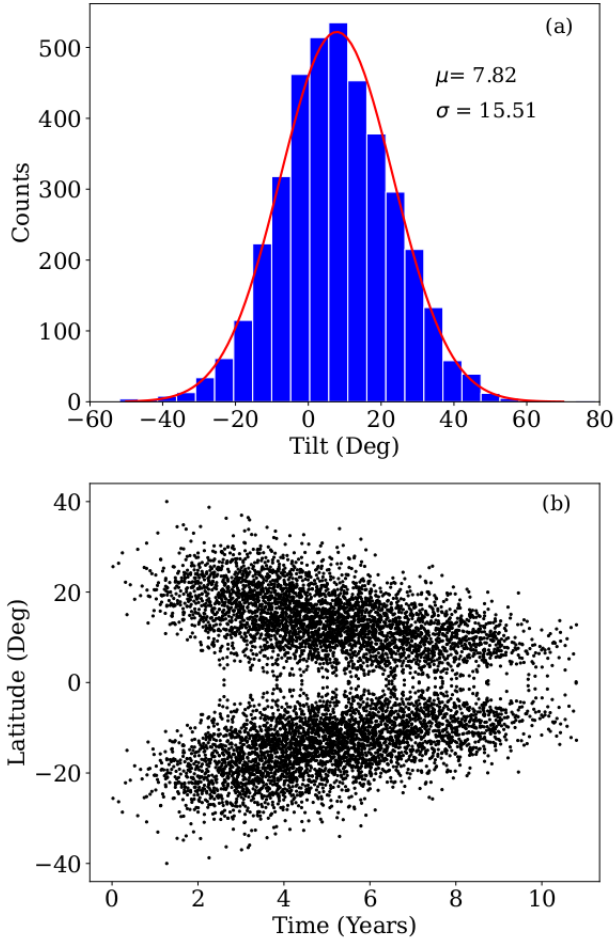
Figure 3. (a) The distribution of BMR tilt with mean = 7.82° and scatter σ = 15.51° as consistent with observations (Wang et al. 2015) and used in our study. (b) Time-latitude distribution of synthetic BMR for one cycle generated using the algorithm described in §2.2.

η_t of order 10^{12}cm^2 s^{-1} (4.5×10^{12}cm^2 s^{-1}for $r \geq 0.956R$ and 1.5×10^{12}cm^2 s^{-1} below) throughout the whole CZ. Below the CZ, the magnitude of the diffusivity is reduced by about four orders of magnitude; see Eq. 4 of Karak & Miesch (2017).

A crucial part of this model is the Spotmaker algorithm, which places a BMR on the surface when certain conditions are satisfied. The first condition for generating a BMR is that the magnetic field strength at the base of CZ must exceed a critical field strength B_c. We have made B_c latitude dependent such that it makes BMR emergence difficult at high latitudes and it helps the model BMRs to be consistent with the observations (Karak 2020). The second condition is the time delay between successive BMR emergence. After the first BMR eruption, the time delays for the subsequent eruptions are taken randomly from the observed log-normal distribution as shown in Fig. 2(a), which follows the profile:

$$P(\Delta) = \frac{1}{\sigma_d \Delta \sqrt{2\pi}} \exp\left[\frac{-(\ln \Delta - \mu_d)^2}{2\sigma_d^2} \right] \qquad (3)$$

Where σ_d and μ_d are specified as, $\sigma_d^2 = \frac{2}{3}\left[\ln \tau_s - \ln \tau_P \right]$ and $\mu_d = \sigma_d^2 + \ln \tau_P$. Here $\tau_P = 0.8$ and $\tau_s = 1.9$ and Δ is the time delay between two successive BMRs (normalized to one day).

Now we have to specify the properties of BMRs (tilt, flux, and separation) in this model. We take a log-normal distribution of flux that is close to the observed one as shown in Fig. 2(b).

$$P(\phi) = \phi_0 \frac{1}{\sigma_\phi \phi \sqrt{2\pi}} \exp\left[\frac{-(\ln \phi - \mu_\phi)^2}{2\sigma_\phi^2} \right] \qquad (4)$$

where $\phi_0 = 1$, $\mu_\phi = 51.2$, and $\sigma_\phi = 0.77$. We have specified the BMR field strength at the surface as 3 kG. For the separation of BMRs, we choose the half distance between the centers of two spots of BMR to be 1.5 times the radius of the spot. The radius of the BMRs is determined based on the log-normal distribution of the flux and is given as, $r = \sqrt{\frac{\phi}{B_s \pi}}$, where B_s is the surface field. For the tilt angle of BMRs, we follow the standard Joy's law (Dasi-Espuig et al. 2010; Stenflo & Kosovichev 2012; Sreedevi et al. 2024):

$$\delta = \delta_0 \cos \theta + \delta_f, \qquad (5)$$

where θ is co-latitude, $\delta_0 = 35°$, and δ_f includes fluctuations in the tilt around Joy's law which follows a Gaussian distribution with $\sigma_\delta \approx 15°$ (e.g., Sreedevi et al. 2024). After giving a scatter of $\sigma_\delta \approx 15°$, we have found 30 – 35% BMRs are anti-Hale and anti-Joy. We have ensured that 25 – 30% of total BMRs would be anti-Joy, and about 8% would be anti-Hale, as observational results suggest. The distribution of the tilt δ for a cycle is shown in Fig. 3(a).

Further, we discuss the nonlinearity needed to limit the growth of the magnetic field. In our model, the latitude-dependent BMR threshold introduces a nonlinearity the so-called latitude quenching (Jiang 2020; Karak 2020). This helps to stabilize the growth of the magnetic field in our model. In addition to this, we include a magnetic field-dependent quenching of the form: $1/\left[1 + (B/B_0)^2\right]$ in the tilt of BMR (tilt-quenching), inspired by the observations (Jha et al. 2020); for more details about the model see Karak & Miesch (2017).

2.2 Deposition of synthetic BMRs in STABLE

Now we discuss how instead of using the SpotMaker algorithm, we can feed synthetic BMR data into STABLE to operate this as SFT model. Following Jiang et al. (2018), we develop a synthetic BMR generation code (SBMR Code) to produce smoothed monthly synthetic BMR data. This can be described by the following equation.

$$\overline{F}_{sm}(t) = f_2(t) + \overline{\Delta r(t)} f_2(t). \qquad (6)$$

Here

$$f_2(t) = \frac{at^3}{\exp\left[\frac{t^2}{b^2} \right] - c}, \qquad (7)$$

where t is time in month, $a = \left(\frac{S_n}{9072.8} \right)^{\frac{1}{0.706}}$ with S_n the amplitude of the sunspot cycle, $b = 27.12 + \left(\frac{25.15}{1000a} \right)^{\frac{1}{4}}$, and $c = 0.71$.
When $t < 72$ months,

$$\overline{\Delta r(t)} = 8.68 \exp\left(\frac{-z_1^2}{2} \right) \qquad (8)$$

with $z_1 = \frac{t-200.44}{45.86}$.
When $72 \leq t \leq 108$ months, then

$$\overline{\Delta r(t)} = 2.64 \exp\left(\frac{-z_2^2}{2} \right) \qquad (9)$$

with $z_2 = \frac{t-149.0}{27.31}$.

Finally in the last phase, when $t > 108$ months, the synthetic BMR follows the given profile:

$$\overline{F}_{sm}(t) = f_2(t). \tag{10}$$

After getting synthetic BMRs, we need to specify the properties of these BMRs. The mean latitude of the BMRs distribution λ_n depends on the cycle strength S_n and it follows the profile:

$$\lambda_n(t) = \left[26.4 - 34.2\frac{t}{T_{cy}} + 16.1 \left(\frac{t}{T_{cy}} \right)^2 \right] \frac{\overline{\lambda}_n}{14.6}, \tag{11}$$

where $\overline{\lambda}_n = 12.2 + 0.015 S_n$ and T_{cy} is the cycle period in month. The scatter in latitude distribution obeys a Gaussian profile with σ defined as:

$$\sigma = \left[0.14 + 1.05\frac{t}{T_{cy}} - 0.78 \left(\frac{t}{T_{cy}} \right)^2 \right] \lambda_n(t). \tag{12}$$

We consider synthetic BMR emergence symmetric in both hemispheres, and the longitudinal distribution of BMRs are random. The BMR eruption time delay is taken randomly within a month. The time-latitude distribution of the resultant synthetic BMR data for one cycle is shown in Fig. 3(b). The flux and tilt are taken from the same prescriptions as discussed above (equations (4) and (5)).

3 RESULTS AND DISCUSSION

We first quantify the effect of randomness due to distributions in BMR properties on the polar field using the STABLE dynamo model as SFT. Later we shall measure the variability of the solar cycle using the STABLE as a dynamo model.

3.1 Variation in the polar field

We feed synthetic BMR data for one cycle (of about 11 years long) in STABLE and perform simulations by operating it as SFT model with random variation in different BMR properties. For the statistical reliability of the result, we have repeated each case for 30 different realizations of the random number. As a reference case, we first perform a simulation without adding any random component in the BMR properties. To address the variability in the polar field arising from different fluctuating parameters of BMRs, we calculate the standard deviation σ_{pol} from 30 realizations in each case relative to the reference polar field. We also calculate the relative variability attributed from the distributions of various BMR parameters, denoted as $\sigma_{pol}/\sigma_{pol}^{com}$, where σ_{pol} represents the standard deviation due to individual BMR parameters (e.g., for time delay $\sigma_{pol} = 0.012\,G$), and σ_{pol}^{com} represents the standard deviation resulting from the combined fluctuations which is $2.39\,G$; see Table 1. For the quantification of the polar field, we compute the remnant magnetic flux strength from $55°$ latitude to the pole in the northern hemisphere. It is worth mentioning that our focus is solely on assessing the comparative effects of various irregular BMR parameters on the polar field. Consequently, we make two hemispheres symmetric. However, Nagy et al. (2017) studied the hemispheric asymmetry due to a single rough BMR and in our dynamo simulations, we do not impose hemispheric asymmetry. The variation of this polar field for the reference case is shown by the black curve in all the Figures 4 – 5.
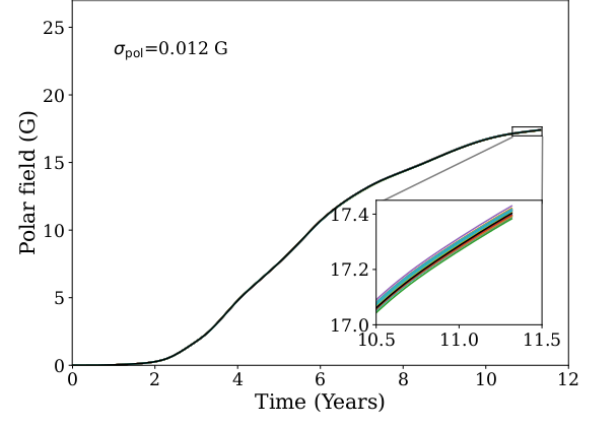

Figure 4. The plot shows the variation in the polar field arises from the randomness due to the distribution in the time delay. The black curve is showing a reference polar field in the plot (see inset for the zoomed-in view).

Table 1. Mean μ and standard deviation σ of the distribution of various BMR parameters (2nd column), variability in the polar field σ_{pol} (3rd column) and the relative possible percentage variability (4th column) produced in the polar field due to different individual fluctuation parameters of the BMRs relative to the combined fluctuations (Fig. 5(d); $\sigma_{pol}^{com} = 2.39\,G$).

Variable parameters	Distribution (μ, σ)	σ_{pol} (G)	Relative % variability
Time delay	0.35, 0.76	0.012	0.5%
Latitude	equations (11) and (12)	0.330	13.8%
Flux	51.2, 0.77	0.961	40.2%
Tilt scatter	7.82°, 15.51°	1.624	68.7%

3.1.1 Due to the distribution in BMR time delay

The time evolutions of the polar fields obtained from the simulations with the different realizations of the time delay are shown by different colors in Fig. 4. We find that these curves deviate only negligibly from the reference polar field (see black curve and the inset) and the standard deviation from the reference polar field is $\sigma_{pol} = 0.012\,G$; see Table 1. The reason for the tiny changes in the polar field is the following. The most probable time delay of the BMR emergence rate is less than a day (mode of the distribution is 0.8 days and mean is 1.9 days; see Fig. 2(a) and the probability decreases with increasing the time delay. When the time delay is 10 days, the probability of the BMR emergence is less than 1%. In contrast, the polar field takes about 1 to 2 years to reach the pole from the active latitude belt where it is formed. Hence, the variation in the polar field caused by the variation in the time delay is smoothed out by the time it reaches the pole and we observe only a negligible variation. We note that when we performed different simulations at different realizations of random delay, we kept the total number of BMRs the same in one month. Instead of this, if we increase this time to six months, then we also find a tiny variation in the polar field with respect to the reference case. Hence, based on these simulations, we conclude that the randomness in the time delay introduces only a slight variation in the polar field.

3.1.2 Due to the distribution in BMR flux

Now, we analyze the result of the simulations with variation in the BMR flux, which is lognormally distributed as mentioned in equation
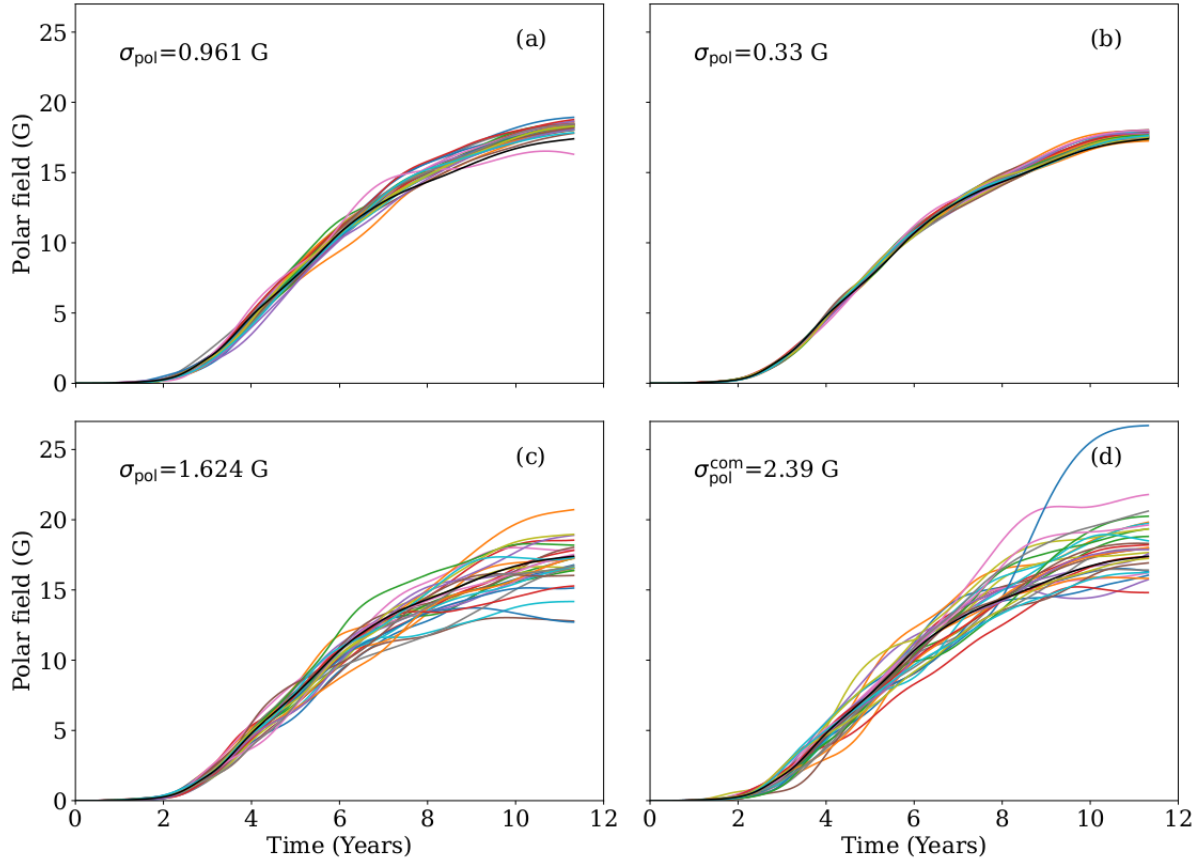
Figure 5. Format of each panel is the same as Fig. 4, but shows the evolution of polar field from simulations with distribution in (a) BMRs flux (with σ of distribution 0.77), (b) BMRs latitude (with σ of the distribution given by equation (12)), (c) BMR tilt (with distribution $\sigma = 15.51°$), and (d) all four BMR parameters.

(4) of §2, keeping all other parameters of the BMR invariant. For 30 realizations, the total flux of sunspots in a solar cycle is considered a fixed value of $8.93 \times 10^{25} Mx$. Fig. 5 (a) shows the variation of the polar field for this case. Now we observe a noticeable variation in the evolution of the polar field. The standard deviation from the reference polar field is found to be $\sigma_{pol} = 0.961 \, G$. A variation, in this case, is expected because the contribution to the polar field in a given hemisphere from decayed active region flux would be proportional to the total hemispheric active region flux (Kitchatinov & Olemskoy 2011; Petrie 2015). Moreover, Shiota et al. (2012) studied that the net polar flux is also affected by the number and size of the large flux concentrations, which qualitatively agrees with our findings. Therefore, the variation in the BMR flux is one cause of variation in the polar field.

3.1.3 Due to the distribution in the BMR latitude

Variation in the latitude distribution of BMR also gives a variation in the polar field strength ($\sigma_{pol} = 0.33 \, G$). This is shown in Fig. 5(b), in which we present the time evolution of the polar field from simulations at different realizations of the BMR latitudes following the same distribution. We note that the separation of the leading and trailing poles of the BMRs remains unchanged; only the mean (of leading and trailing) latitude of the BMR changes randomly in each cycle. While changing the mean latitude, the tilt is also changed according to Joy's law (equation (5)); however, the fluctuations in tilt as param-

eterized by δ_f remain the same in all simulations. Thus arguably, the variation that we observe in Fig. 5(b) is the combined effect of latitude and tilt. We further note that we keep the mean and spread of the latitude distribution of BMRs the same for all cycles and vary only the individual position of BMR randomly (equations (11) and (12)). Thus, our investigation differs from Baumann et al. (2004) who studied the impact of BMR emergence latitude by changing the mean and spread of the latitude band. Despite the methodological differences, our results qualitatively align with Baumann et al. (2004) findings, supporting the conclusion that changes in the latitude of active regions influence the polar field's strength. A variation in the polar field due to a change in the BMR latitude is expected because when BMRs appear at low latitudes, the cross-equatorial cancellation is much more effective than the BMRs which appear at higher latitudes (Durrant et al. 2004; Jiang et al. 2015; Pal et al. 2023), which has been demonstrated in Fig. 1. Moreover, Jiang et al. (2014); Karak & Miesch (2018) showed that the latitudinal variation of BMRs affects the polar field strength (also see Mordvinov et al. 2022). We note that in our case, the variation in the polar field is less because the mean and the width of the latitude distribution remain the same in all the simulations, while in the observed solar cycle, these vary with the cycle strength. Thus, our study shows that even when we keep the mean latitudinal distribution of the BMR the same and vary the individual latitude of the BMR, we find a noticeable variation in the polar field.
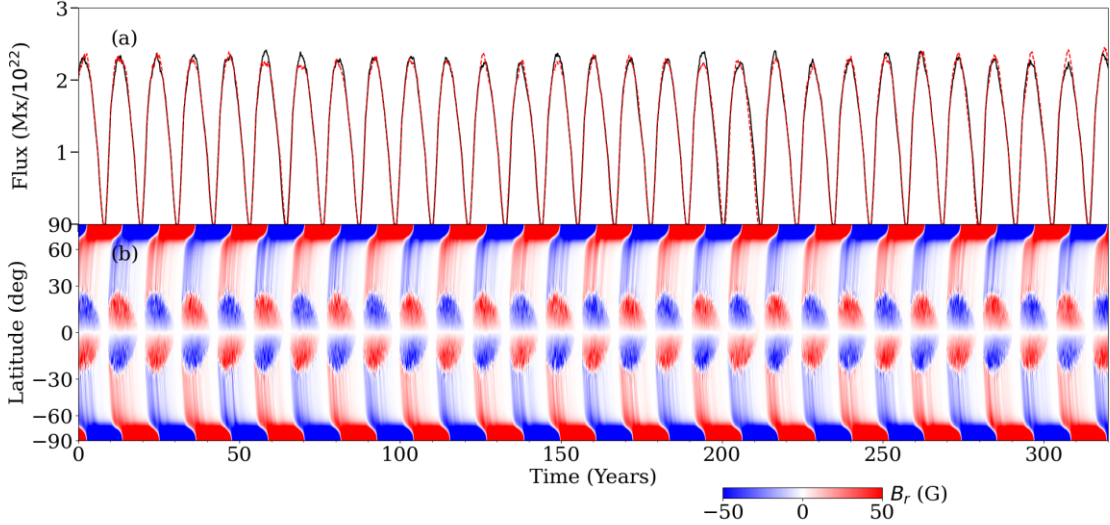
Figure 6. Temporal variations of (a) the monthly total flux of BMRs (red/black: north/south) and (b) the azimuthal-averaged surface radial field from the simulations in which the time delay in BMR eruption is randomly taken from a distribution.

3.1.4 *Due to the distribution in BMR tilt around Joy's law*

Now, we will demonstrate the effect of the tilt scatter of BMR on the polar field. We computed the tilt of BMR using equation (5) i.e., Joy's law with Gaussian scatter captured by δ_f. In each simulation, δ_f changes randomly while keeping the distribution same. Fig. 5 (c) shows the effect of tilt scatter on the polar field variation ($\sigma_{\mathrm{pol}} = 1.624\ G$). As in the Babcock–Leighton process, it is the tilt which makes the generation of the poloidal field possible in the Sun; any change in the tilt can certainly produce variation in the poloidal field. Particularly when we have a wrongly tilted BMR (anti-Joy and anti-Hale), it produces an opposite polarity field (e.g., Nagy et al. 2017; Mordvinov et al. 2022). Recently, Pal et al. (2023) also showed that the emergence timing, relative numbers, latitude distribution, and flux content of anomalous active regions significantly impact the reversal timings and strength of the dipole moment; also see (Golubeva et al. 2023; Biswas et al. 2023b). Furthermore, Jiang et al. (2015) also mentioned that the cause of the weaker cycle 24 is the wrong-tilted BMR (anti-Hale and anti-Joy) at the lower latitude, which decreases the polar field strength. In our model, we have included about 30 to 35% anti-Hale and anti-Joy BMRs (consistent with observations). These anti-Hale and anti-Joy BMRs have opposite tilts than regular BMRs and generate the opposite polarity field. This opposite polarity field brings about a large fluctuation in the polar field of our simulation. Previously Upton et al. (2021) also found that increasing the tilt scatter around Joy's law significantly increases the change in the polar axial dipole from one cycle to the next. By comparing the simulations presented in the previous three sections with randomness in BMR time delay, flux, latitude, and tilt, we conclude that the tilt scatter produces maximum variation in the polar field. For comparative variability in the polar field due to these parameters (see Table 1).

3.1.5 *Due to combined fluctuations*

Now we measure the polar field variation due to the combined effect of all the fluctuations, i.e., the variations in tilt, time delay, flux, and latitude. This replicates the realistic scenario. The fluctuations due to

the distributions of time delay, flux, latitude and tilt are captured precisely in the same proportion (distribution) as they were considered in the individual cases performed above. Fig. 5 (d) shows the polar field variation in this case. We find that in this case, the variation in the net polar field strength is highest ($\sigma_{\mathrm{pol}} = 2.39\ G$, which we define as $\sigma_{\mathrm{pol}}^{\mathrm{com}}$). Maximum variation is expected because all individual random effects can contribute additively.

3.2 Variation in the solar cycle

Now we study the variability of the solar cycle due to irregular properties of BMR by operating STABLE in default mode, i.e., as a dynamo model. For this, we consider three cases: (i) irregular time delay in the BMR eruption, (ii) irregular BMR flux, and (iii) scatter in BMR tilt angle around Joy's law. The incorporation of fluctuations in different BMR properties in the dynamo model is exactly the same as done in the study of polar field variation, which are explained in §2. To be more specific, the time delay, flux and tilt distributions are taken from equations (3), (4), and (5), respectively. We note that to study solar cycle variation, we are not considering the case of the variation in the BMR latitude separately because it is not trivial to vary BMR latitude randomly by hand in the dynamo mode of this model. When the cycle strength varies, the mean latitude of BMR varies; hence it will be captured when cycle strength varies due to variation in the polar field caused by fluctuations in BMR properties. In STABLE, at every numerical timestep, a BMR latitude is chosen randomly out of the latitude points where the azimuthal field exceeds the threshold which is latitude-dependent. Moreover, we have seen in §3.1.3 (Fig. 5(b)) that in the case of variation in latitude due to its distribution, the variation in the polar field is less compared to the variations in the tilt and flux and thus we are not performing any simulations for this case.

Fig. 6 shows the solar cycle variability produced by the random time delay in BMR emergence. The variation is measured in terms of the monthly value of the BMR flux and the surface radial field as the function of time. We find that the variability in the solar cycle in both hemispheres is negligible. In the polar field evolution §3.1.1, we have already seen that the random time delay in BMR eruption
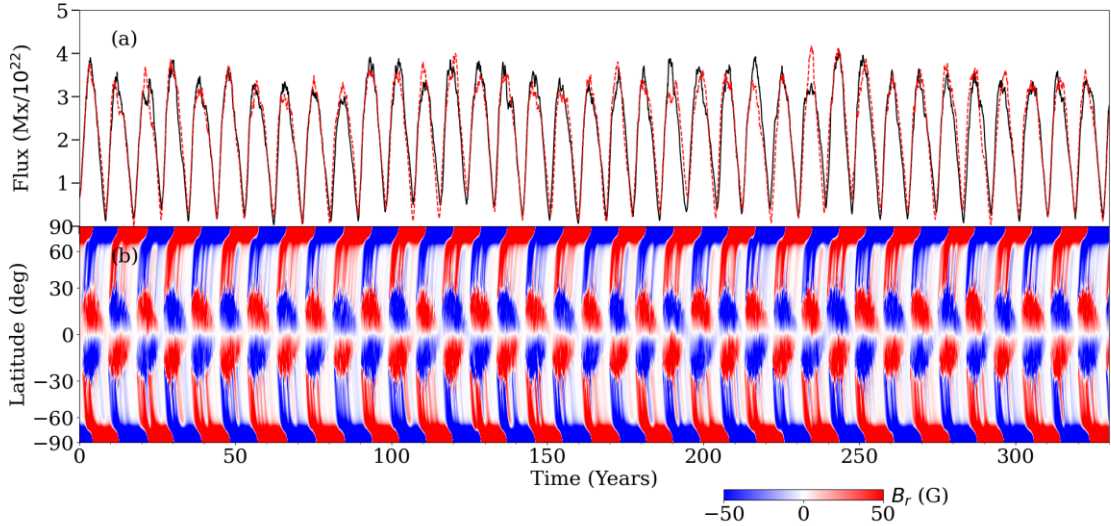
Figure 7. Same as Fig. 6 but from the simulation in which BMR flux is taken from a distribution.
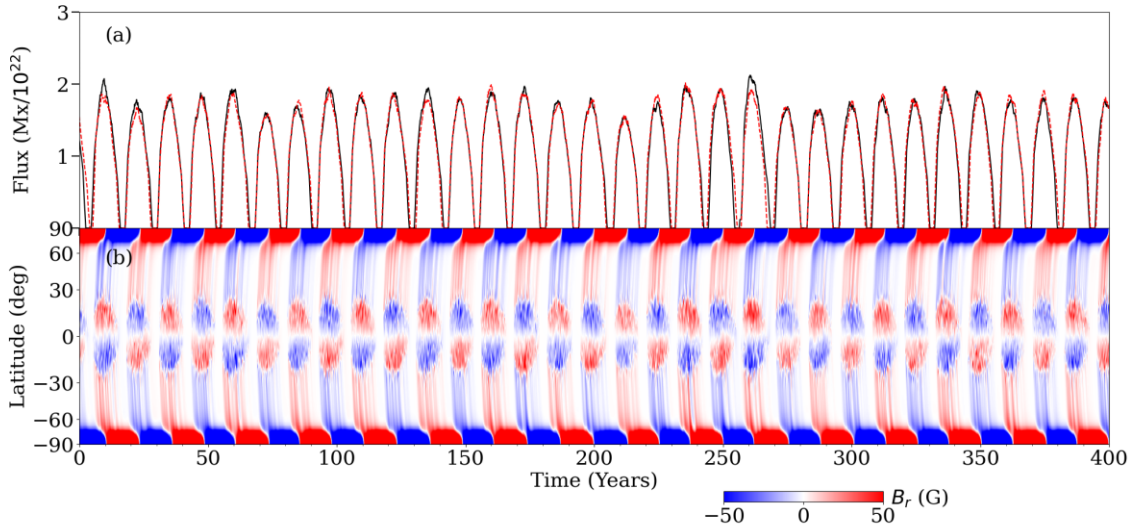

Figure 8. Same as Fig. 6 but from the simulation in which the tilt is randomly taken from a distribution.

causes a negligible variation in the polar field. In the context of Babcock–Leighton dynamo, the poloidal field gives toroidal field, which eventually produces BMRs on the solar surface. Therefore, a tiny variation in the polar field is expected to cause a tiny variation in the next solar cycle. While this expectation is based on the dynamo mechanism (e.g., Charbonneau & Barlet 2011; Kumar et al. 2021) and the observations (Muñoz-Jaramillo et al. 2013), if the dynamo operates in the chaotic region (much above the critical transition), even a small change in the polar field can lead to a large change in the solar cycle. However, it is important to note that our model does not operate within that specific region, and thus, such effects are not accounted for in our model. In summary, the simulation performed in this case indicates that irregular rate of BMR emergence does not produce significant variation in the solar cycle.

However, when we perform the dynamo simulation with the variation in BMR flux, we observe a considerable amount of long-term modulation in the solar cycle as seen in Fig. 7. This is expected given

the fact that it produces a significant variation already in the polar field as seen in §3.1.2. Next, when we consider the scatter in BMR tilt around Joy's law, we again find a large amount of variation in the solar cycle as seen in Fig. 8. Again this result is congruous with the expectation that a considerable variation in the polar field is observed with the tilt scatter. Previous studies have also shown that the scatter in BMR tilt can produce large variations in the solar cycle, including grand minima and grand maxima (Lemerle & Charbonneau 2017; Nagy et al. 2017; Karak & Miesch 2017, 2018).

Now we perform two other simulations by including all the fluctuations mentioned above individually i.e., variation in time delay, flux, and tilt. The basic difference between these two simulations is the only time delay. In one simulation, the time delay is magnetic field independent (Fig. 9), while in another it is magnetic field dependent (Fig. 10). To make the time delay magnetic field dependent, we make the following changes in the time delay parameters for both
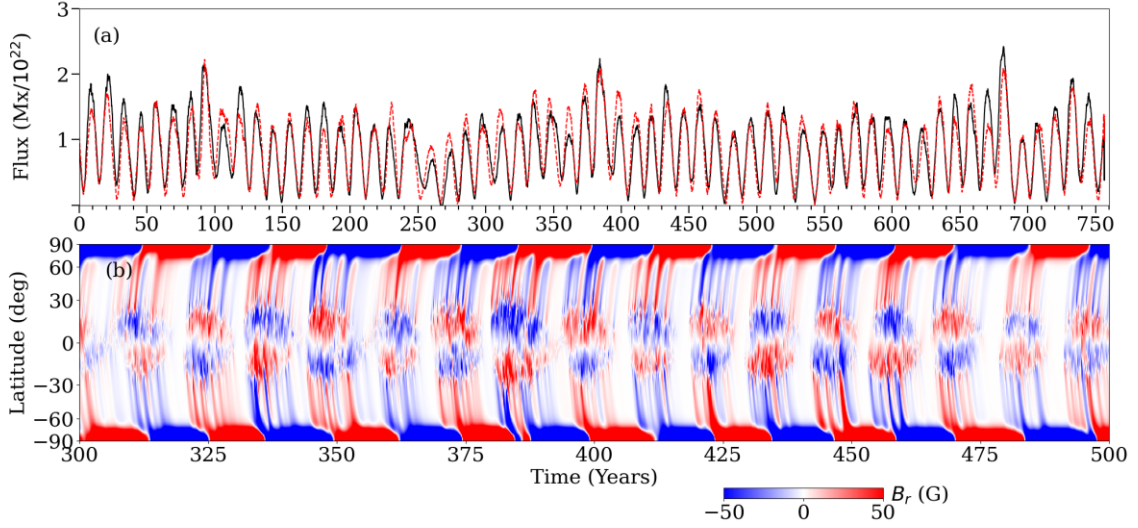
Figure 9. Same as Fig. 6 but from simulations including distributions in all BMR properties (i.e., time delay, flux, latitude, and tilt) and the time delays are magnetic field independent.
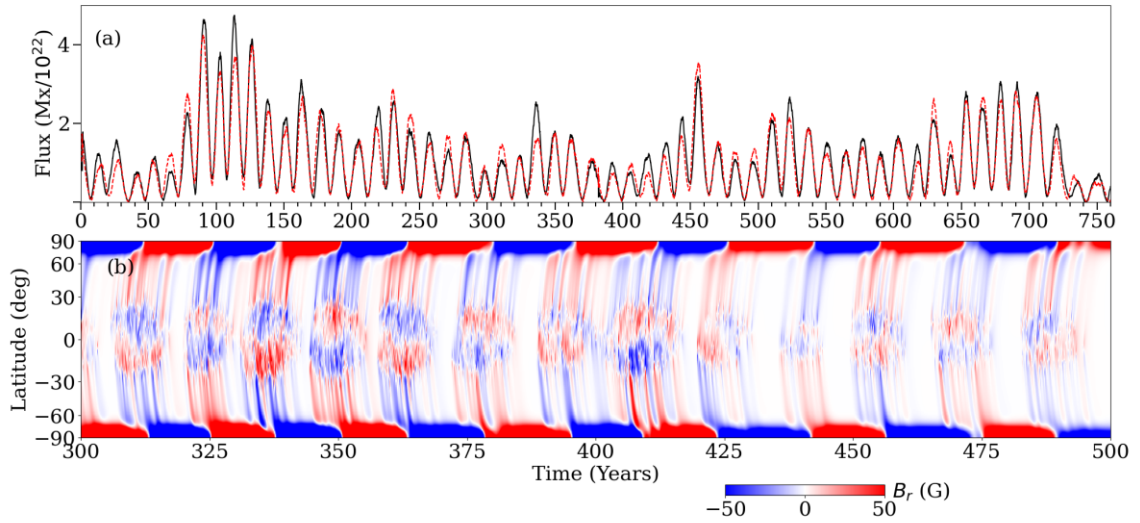

Figure 10. Same as Fig. 9 but with magnetic field-dependent time delay.

hemispheres:

$$\tau_p = \frac{2.2}{1 + \left[\frac{B_b}{400}\right]^2}, \quad \text{and} \quad \tau_s = \frac{20}{1 + \left[\frac{B_b}{400}\right]^2}, \tag{13}$$

where B_b is the azimuthal-averaged toroidal magnetic field in a thin layer spanning from $r = 0.715R$ to $0.73R$ at approximately $15°$ latitude.

We find more variability and grand minima-like appearance when the time delay is magnetic field dependent. However, in the magnetic field independent case, we observe a few triple reversals of the polar field; see reversal in the southern hemisphere between $375 - 400$ years in Fig. 9(b). We find triple reversal events in the magnetic field-independent time delay case because in this case, the emergence rate of BMRs does not change much over the solar cycle, while in the magnetic field-dependent case, it varies largely with the solar cycle—becoming highest around the solar maxima and lowest around the solar minima (because in this case the time delay is magnetic field dependent and varies according to the magnetic field strength). Therefore, in the magnetic field-independent case, the emergence rate around the cycle maxima is less (compared to the magnetic field-dependent case), and as the BMR number is less, the effect of tilt scatter (the anti-Joy and anti-Hale BMR) is statistically more prominent. However, in the magnetic field-dependent case, the effect of tilt scatter largely cancels out due to the relatively large number of BMR emergences at the times of cycle maxima and this does not lead to triple reversals. Moreover, observations and models (Mordvinov et al. 2022) both reveal that the occurrence probability of triple reversal events is maximum around the time of solar cycle maxima.

Further, magnetic field-dependent and independent time delays produce variability in the solar cycle in a different way. Since grand minima and maxima-like events are more probable in the magnetic field-dependent time delay case and the morphology of the magnetic

field better resembles the solar observation in this case, the magnetic field-dependent time delay case is more favorable with observation. Indeed, the distribution of the time delay in the observation varies with the solar cycle—becoming narrower during solar maximum and thus it is magnetic-field dependent.

4 CONCLUSIONS

In this study, we have utilized the 3D STABLE dynamo model to quantify the relative variations of the polar field and the solar cycle due to the stochastic properties of BMRs in the poloidal field generation (Babcock–Leighton process). We, for the first time, showed that our dynamo model can reproduce the most robust feature, namely the variation of the generated axial dipole moment with the latitude of BMR, as found in SFT models (e.g., Jiang et al. 2014). Thus, it gives some confidence on the applicability of the results of the dynamo model to observations. Next we present the distributions of the flux and time delay of BMRs obtained by tracking them from the high-resolution magnetograms. Guided by these observations that the BMR properties follow distributions, we have studied the variations that arise from the distributions in the following processes: (i) time delay in BMR emergence, (ii) BMR flux, (iii) BMR latitude, and (iv) BMR tilt angle. While earlier studies presented significant disturbance in the polar field due to the scatter in the BMR tilt around Joy's law (e.g., Jiang et al. 2014; Karak & Miesch 2017), anomalous BMRs (Nagy et al. 2017; Pal et al. 2023), changes in the flux and latitudinal positions of BMRs (Baumann et al. 2004; Hazra et al. 2017; Bhowmik & Nandy 2018; Pal et al. 2023), here we presented a comparative analysis of the variation of the polar field and the solar cycle strength using the same input and the same model (STABLE), operating as SFT and dynamo modes. Unlike previous studies, we have kept the cycle strength same, and thus the mean and width of the distributions of the tilts, latitudes, and fluxes of BMRs of the cycles are the same, and we only varied the individual properties of BMRs, keeping their distributions the same. The most surprising result of our study is that the time delay and latitude variations produce only little variations in the mean polar field of the cycle (and thus the cycle strength). A relatively large variation is observed due to distribution in the flux and the largest variability appears due to scatter in the BMR tilt; see Table 1. The combined effects of the distributions of all parameters of the BMRs on the polar field and the solar cycle are obviously the highest, and they are sufficient to reproduce a large spectrum of the observed modulation in the solar cycle and the magnetic field, including producing grand minima and maxima, and triple reversals of the polar field (Mordvinov et al. 2022). In agreement with previous results, our study suggests that the irregular properties of BMR as observed in the forms of their respective distributions are the major causes of the observed variability in the polar field and the solar cycle. Moreover, our simulations show that the magnetic field-dependent time delay of BMR emergence produces more realistic features of the magnetic cycle, and this is consistent with observation as well.

ACKNOWLEDGEMENTS

DATA AVAILABILITY

For all analyses, we have used data produced from the STABLE dynamo model and synthetic BMR code. Data from our models and the analysis codes can be shared upon a reasonable request.

REFERENCES

Babcock H. W., 1961, ApJ, 133, 572
Baumann I., Schmitt D., Schüssler M., Solanki S. K., 2004, A&A, 426, 1075
Beer J., Tobias S., Weiss N., 1998, Sol. Phys., 181, 237
Bhowmik P., Nandy D., 2018, Nature Communications, 9, 5209
Bhowmik P., Jiang J., Upton L., Lemerle A., Nandy D., 2023, Space Sci. Rev., 219, 40
Biswas A., Karak B. B., Cameron R., 2022, Phys. Rev. Lett., 129, 241102
Biswas A., Karak B. B., Usoskin I., Weisshaar E., 2023a, Space Sci. Rev., 219, 19
Biswas A., Karak B. B., Kumar P., 2023b, MNRAS, 526, 3994
Cameron R., Schüssler M., 2015, Science, 347, 1333
Cameron R. H., Schüssler M., 2016, A&A, 591, A46
Cameron R. H., Schmitt D., Jiang J., Işık E., 2012, A&A, 542, A127
Cameron R. H., Dasi-Espuig M., Jiang J., Işık E., Schmitt D., Schüssler M., 2013, A&A, 557, A141
Cameron R. H., Jiang J., Schüssler M., 2016, The Astrophysical Journal Letters, 823, L22
Charbonneau P., 2020, Living Reviews in Solar Physics, 17, 4
Charbonneau P., Barlet G., 2011, Journal of Atmospheric and Solar-Terrestrial Physics, 73, 198
Choudhuri A. R., Chatterjee P., Jiang J., 2007, Physical Review Letters, 98, 131103
Dasi-Espuig M., Solanki S. K., Krivova N. A., Cameron R., Peñuela T., 2010, A&A, 518, A7
Durrant C. J., Turner J. P. R., Wilson P. R., 2004, Sol. Phys., 222, 345
Golubeva E. M., Biswas A., Khlystova A. I., Kumar P., Karak B. B., 2023, MNRAS, 525, 1758
Gurgenashvili E., et al., 2016, The Astrophysical Journal, 826, 55
Hale G. E., Ellerman F., Nicholson S. B., Joy A. H., 1919, ApJ, 49, 153
Hazra G., Choudhuri A. R., Miesch M. S., 2017, ApJ, 835, 39
Howard R. F., 1991, Sol. Phys., 136, 251
Jha B. K., Karak B. B., Mandal S., Banerjee D., 2020, ApJ, 889, L19
Jiang J., 2020, ApJ, 900, 19
Jiang J., Cameron R. H., Schüssler M., 2014, ApJ, 791, 5
Jiang J., Cameron R. H., Schüssler M., 2015, ApJ, 808, L28
Jiang J., Wang J.-X., Jiao Q.-R., Cao J.-B., 2018, The Astrophysical Journal, 863, 159
Jouve L., Proctor M. R. E., Lesur G., 2010, A&A, 519, A68
Karak B. B., 2020, The Astrophysical Journal Letters, 901, L35
Karak B. B., 2023, Living Reviews in Solar Physics, 20, 3
Karak B. B., Cameron R., 2016, ApJ, 832, 94
Karak B. B., Choudhuri A. R., 2011, MNRAS, 410, 1503
Karak B. B., Miesch M., 2017, ApJ, 847, 69
Karak B. B., Miesch M., 2018, ApJ, 860, L26
Karak B. B., Jiang J., Miesch M. S., Charbonneau P., Choudhuri A. R., 2014, Space Sci. Rev., 186, 561
Karak B. B., Mandal S., Banerjee D., 2018, ApJ, 866, 17
Kitchatinov L. L., Olemskoy S. V., 2011, Astronomy Letters, 37, 656
Kitchatinov L. L., Mordvinov A. V., Nepomnyashchikh A. A., 2018, A&A, 615, A38
Kumar P., Nagy M., Lemerle A., Karak B. B., Petrovay K., 2021, ApJ, 909, 87

Kumar P., Biswas A., Karak B. B., 2022, MNRAS, 513, L112

Leighton R. B., 1964, ApJ, 140, 1547

Lemerle A., Charbonneau P., 2017, ApJ, 834, 133

Makarov V. I., Fatianov M. P., Sivaraman K. R., 1983, Sol. Phys., 85, 215

Mandal S., Karak B. B., Banerjee D., 2017, ApJ, 851, 70

Martin-Belda D., Cameron R. H., 2017, A&A, 597, A21

McClintock B. H., Norton A. A., 2016, ApJ, 818, 7

McClintock B. H., Norton A. A., Li J., 2014, ApJ, 797, 130

Miesch M. S., Dikpati M., 2014, ApJ, 785, L8

Miesch M. S., Teweldebirhan K., 2016, Advances in Space Research, 58, 1571

Mordvinov A. V., Karak B. B., Banerjee D., Golubeva E. M., Khlystova A. I., Zhukova A. V., Kumar P., 2022, MNRAS, 510, 1331

Muñoz-Jaramillo A., Dasi-Espuig M., Balmaceda L. A., DeLuca E. E., 2013, ApJ, 767, L25

Nagy M., Lemerle A., Labonville F., Petrovay K., Charbonneau P., 2017, Sol. Phys., 292, 167

Nagy M., Lemerle A., Charbonneau P., 2020, Journal of Space Weather and Space Climate, 10, 62

Pal S., Bhowmik P., Mahajan S. S., Nandy D., 2023, The Astrophysical Journal, 953, 51

Parker E. N., 1955, ApJ, 121, 491

Petrie G. J. D., 2015, Living Reviews in Solar Physics, 12, 5

Petrovay K., 2020, Living Reviews in Solar Physics, 17, 2

Petrovay K., Nagy M., Yeates A. R., 2020, Journal of Space Weather and Space Climate, 10, 50

Priyal M., Banerjee D., Karak B. B., Muñoz-Jaramillo A., Ravindra B., Choudhuri A. R., Singh J., 2014, ApJ, 793, L4

Rieger E., Share G. H., Forrest D. J., Kanbach G., Reppin C., Chupp E. L., 1984, Nature, 312, 623

Schatten K. H., Scherrer P. H., Svalgaard L., Wilcox J. M., 1978, Geophys. Res. Lett., 5, 411

Schou J., et al., 1998, ApJ, 505, 390

Sheeley N. R. J., 1966, ApJ, 144, 723

Shiota D., Tsuneta S., Shimojo M., Sako N., Orozco Suárez D., Ishikawa R., 2012, ApJ, 753, 157

Sivaraman K. R., Gokhale M. H., Sivaraman H., Gupta S. S., Howard R. F., 2007, ApJ, 657, 592

Solanki S. K., Usoskin I. G., Kromer B., Schüssler M., Beer J., 2004, Nature, 431, 1084

Solanki S. K., Wenzler T., Schmitt D., 2008, A&A, 483, 623

Sreedevi A., Jha B. K., Karak B. B., Banerjee D., 2023, ApJS, 268, 58

Sreedevi A., Jha B. K., Karak B. B., Banerjee D., 2024, ApJ, p. arXiv:2403.09229

Stenflo J. O., Kosovichev A. G., 2012, ApJ, 745, 129

Svalgaard L., 2013, Journal of Space Weather and Space Climate, 3, A24

Temmer M., 2021, Living Reviews in Solar Physics, 18, 4

Teweldebirhan K., Miesch M., Gibson S., 2024, Solar Physics, 299

Tobias S. M., Brummell N. H., Clune T. L., Toomre J., 1998, ApJ, 502, L177

Upton L., Coddington O., Kopp G., Lean J., 2021, in American Astronomical Society Meeting Abstracts. p. 304.07

Usoskin I. G., 2017, Living Reviews in Solar Physics, 14, 3

Waldmeier M., 1935, Astronomische Mitteilungen der Eidgenössischen Sternwarte Zurich, 14, 105

Waldmeier M., 1955, Ergebnisse und Probleme der Sonnenforschung.

Wang Y.-M., Sheeley N. R., 2009, ApJ, 694, L11

Wang Y.-M., Colaninno R. C., Baranyi T., Li J., 2015, ApJ, 798, 50

Weiss N. O., Tobias S. M., 2016, MNRAS, 456, 2654

This paper has been typeset from a TeX/LaTeX file prepared by the author.